Unit process energy consumption analysis and models for Electron Beam Melting (EBM): Effects of process and part designs

Unit process energy consumption analysis and models for Electron Beam Melting (EBM): Effects of process and part designs

Vincenzo Lunetto[1], Manuela Galati[1]*, Luca Settineri[1], Luca Iuliano[1]

[1]Department of Management and Production Engineering, Politecnico di Torino, Corso Duca degli Abruzzi 24, 10129 Torino, Italy

* Corresponding author

Email: manuela.galati@polito.it

Ph.: (+39) 0110904569

Abstract

Electron Beam Melting (EBM) has the potentiality of being an effective system in terms of time and energy consumption. Among the different additive manufacturing processes that are available, the EBM process has shown the lowest Specific Energy Consumption (SEC) and the highest average Deposition Rate (DR_a). However, there appears to be a lack of literature on the correlation between SEC and DR_a. Moreover, all the literature studies have only an analysis of the energy efficiency during the melting of the bulk material phase and have adopted a fixed job design. Therefore, the aim of this study has been to fill this gap. The EBM process is decomposed into small substeps and a bottom-up approach is adopted to provide models that can be used to evaluate the energy of each process subphase and to perform an energy characterisation at the unit process level. A black-box approach is applied to provide a new model for the energy efficiency of the EBM process. Different jobs have been designed to analyse the effect of a part and of manufacturing designs. Bulk material, support and lattice structures have been included. The design has therefore been aimed at investigating the effect of the build height, melted area and process themes on energy efficiency. The jobs have been produced using Arcam A2X and Standard Arcam Ti6Al4V powders. According to this research, the architecture of the machine and its control of the process have the main impact on the relationship between SEC and DR_a. The design features of the part and of the job influence the position of the job on this curve and thus the relative energy and time efficiency. Additionally, the empirical approach applied to the machine subunits has highlighted that only a small part of the total energy demand is needed to power the electron beam during the melting phase, while the remaining part guarantees the good machine working conditions.

Keywords: Additive Manufacturing; Electron Beam Melting; Sustainable manufacturing; Energy efficiency.

1. Introduction

Additive Manufacturing (AM) describes a set of manufacturing technologies that allows a part to be manufactured directly, layer by layer, from a 3D CAD model [1]. AM technologies are now considered one of

the most important emerging technologies that have already shown a great potential in several industrial sectors. Electron Beam Melting (EBM) is one of AM processes that is already used for the mass production of metal components in the aerospace and medical fields, because it allows complex structures and excellent materials to be produced easily [2]. EBM is a metal powder bed fusion (PBF) AM process in which an electron beam (EB) is used to selectively melt powder [3]. As EBM process is replacing such traditional processes as casting, a crucial issue concerns the assessment of the sustainability of the process, and thus the environmental burdens associated with the process, which may be highlighted through a life cycle assessment. Preliminary analyses have detected a higher energy demand for AM processes than for subtractive and bulk processes [4,5]. Specific applications of this methodology that considered all the energetic inputs to produce a part by means of EBM processes, from powder production to post-processing, have highlighted that the manufacturing step is one of the main contributions that has to be taken into consideration to calculate the energy demands [6]. The energy efficiency of a manufacturing machine can be measured, at the manufacturing level, by considering the Specific Energy Consumption (SEC). In the presented work, the EBM process is analysed fully from the energetic point of view. The EBM process was initially decomposed into substeps and a bottom-up approach was adopted to provide models for the energy evaluation of each subphase of the process as well as for a characterisation of the unit process level energy. Then, an empirical model of the energy efficiency of the EBM process was developed. Different jobs were designed to analyse the effects of the part and manufacturing design. All feature that can processed by EBM process were included in the study. The design was therefore aimed at investigating the effect of the build height, melted area, nesting along the building direction and process themes on energy efficiency. The jobs and the measurements were performed using Arcam A2X and Standard Arcam Ti6Al4V powders.

2. Literature Review

2.1 EBM process

The EBM process consists of several steps. Initially, the EB preheats the start plate uniformly. A rake system then distributes a uniform powder bed, which is preheated completely by several smooth beam passages at a high beam current and high scan speed. The preheating of both the start plate and the powder bed is run up to a specific temperature, which depends on the material that has to be processed. The preheating of the powder bed consists of two subsequent steps. The powder bed is first uniformly preheated by a series of beam passages. The preheated area corresponds to the maximum rectangular area that contains all the parts that have to be melted. The powder is then further heated in an area that corresponds to a predefined offset of the actual melting zone. The initial preheating is mainly aimed at avoiding the spread of the powder during the melting phase, while the latter one decreases the thermal gradient for the subsequent melting phase. The preheating phase sinters the particles, prevents the so-called smoke effect and creates a neck connection between the particles that improves thermal conductivity [2]. Thanks to this partial sintering, the powder bed has a certain strength [7], the parts can therefore be nested along the building direction and the number and the length of the supports are reduced. Different melting strategies can be used to melt the contour and inner parts of the section

that has to be melted. A MultiBeam™ [8] strategy is generally used for the contour [9], while a hatching strategy is used for the inner part [8]. After the melting phase, an additional step, called postheating [10], is introduced. The aim is to keep the build at the correct temperature. In this step, the layer can either be cooled down or further heated, depending on the total amount of energy supplied during the previous steps [11]. The entire process is performed in a vacuum environment that is generated by turbo molecular pumps [12]. The several heating steps and the vacuum environment guarantee high temperatures and low thermal gradients during the process. Furthermore, after the start of the electron beam, a small amount of inert helium gas is added to avoid the build-up of electrical charges in the powder and to ensure thermal stability of the process. After the build task has been completed, the entire build is cooled down inside the machine to 80°C. The helium pressure is increased during the cooling phase.

The features that can be processed by EBM are usually grouped into support structures, lattice structures and the so-called bulk material. The differences are mainly due to the function of the part and the relative heat distribution during the process. Support and lattice structures are usually characterised by a small melted area. Additionally, the support structures need to be easy to remove manually, and a certain level of brittleness is therefore mandatory. Fleck et al. [13] defined a lattice structure as being a cellular or mesh array, made up of a large number of uniform elements, generated by tessellating a unit cell throughout the space. An elementary lattice cell consists of a certain number of struts, also called lattice struts, that are jointed in one or more nodes. Therefore, a lattice strut is a link between two nodes. In general, different unit cells can be designed by using different lattice struts between the nodes. The cross section of the struts is small and usually comparable with the electron beam spot. Because of their specific geometries and functions, the process parameters for the support and the lattice structure differ from those of the bulk one. A set of process parameters is called a theme. At least three themes are generally used for each material in the EBM process. An additional theme is used for the preheating step. The process parameters for the post heating are usually the same as those used for the second preheating step [14]. The duration of the post-heating (or cooling) is then calculated according to the average beam current to be achieved over the layer.

2.2 Energy efficiency of EBM process

SEC was first introduced for machining processes by [15,16] with the aim of measuring the entire energy input that a machine tool needs to remove a unit mass of material. A similar approach was adopted for injection molding [17] and friction extrusion [18]. SEC can be defined, for AM processes, as the entire energy input that is needed to deposit or melt a unit mass of material. Baumers et al. [19] compared the energy efficiency of Laser Powder Bed Fusion (L-PBF) with that of EBM systems. The comparison was made by producing a job with a single component. An additional job was produced by replicating components until the building platforms of the two machines were completely saturated. Since a saturation along the height of the build chamber was not investigated, the latter experiment only led to the saturation of the building capacity for a height that corresponded to the benchmarking one. Components produced by EBM are attached directly to the start plate without the need to use support structures. The authors highlighted that the EBM technology required less energy than L-PBF because of the thicker layer thickness and the higher energy per unit area provided by

the electron beam. The saturation of the build chamber led to a reduction in SEC for both processes because of the amortisation of the fixed energy terms due to the higher amount of mass. In fact, the impact of the vacuum generation phase and those of the machine presetting and of the cooling phase can be reduced for the EBM process if the build chamber is saturated. These phases can have an impact of up to 26% on the overall energy demand [20]. Kellens et al. [20] computed an SEC value of 375.0 MJ/kg from the work of Paris et al. [21] (Table 1). Baumers et al. [22] carried out a similar study to that of Baumers et al. [19] in which a larger number of AM technologies were considered: EBM and L-PBF for metals and Fused Deposition Modelling (FDM) and Selective Lase Sintering (SLS) for polymers. All the results showed that energy efficiency increased remarkably as a result of a decrease in the SEC parameters once the number of parts in the job had been increased. The SEC value of a single component (Table 1) for the EBM process was 177 MJ/kg, while it dropped to 61 MJ/kg when the start plate was saturated, and this is the lowest value of all the AM processes. Since the volume in the EBM process can also be fully saturated along the building direction, the system energy efficiency can easily be enhanced. Baumers et al. [23] compared EBM and L-PBF, considering the nesting of 5 different components to saturate the machine platform. The EBM machine (Arcam S12) showed a lower energy consumption than the L-PBF one (EOSINT M270). The ratio between the energy and the mass resulting from Baumers's study led to SEC values of 118.46 MJ/kg and 258.56 MJ/kg for Arcam S12 and EOSINT M270, respectively. Baumers et al. [24] distinguished different energy contributions during the EBM process at a layer level: the spreading of the powder bed, preheating and melting. The Arcam A1 machine was analysed under the full capacity, in a similarly way as in Baumers et al. [19,22], using a bulk component. The results on the SEC values agreed with those reported in [19,22] (Table 1). The effect of the complexity of the component shape on the energy demand of EBM was also investigated. The complexity of the job was described in that experiment theme by means of the mean connectivity value (MCV) of each layer. This parameter acts as an indicator of the distance between the different areas that have to be melted which belong to the same cross section of the component. MCV decreases if the cross section of a component has various areas to be melted that are far from each other. The lower MCV is, the higher the complexity of the section. The results showed that there was no correlation between MCV and the energy demand during the melting phase. Baumers et al. [25] proposed models to estimate the time and the energy needed for powder bed-based AM processes. The authors considered each idle time (i.e. atmosphere generation) as well as each fixed time for each layer (i.e. the time necessary to spread the powder layer). The active time and energy were considered as a linear function of the area that had to be melted, and this evidence was supported by the acquired experimental data. Paris et al. [21] compared the environmental impacts of a turbine manufactured by a five axe milling process and by EBM technology. The subsequent finishing operation for the EBM turbine was also included in the analysis. No significant difference was found for the two manufacturing approaches. The higher impact for EBM was found to be due to the powder production, by means of gas atomisation, and the production of the stock material for the milling process. The energy demand of the EBM machine was found to be lower than that of the five axes milling process when the component that had to be manufactured by machining had smaller dimensions than those of the raw material used in the conventional approach. As the

literature review has highlighted, most of the findings about the SEC values derived from Baumers' works represent the state of the art in [4,5,20,25–29]. Another parameter is the Deposition Rate (DR_a) which defines the ratio between the total melted mass (m_{tot}) and the total time (t_{tot}) needed to produce a part (i.e. considering any idle, pre-setting and cooling times) and is expressed by Eq. 1 in kg/h.

$$DR_a = \frac{m_{tot}}{t_{tot}} \qquad (1)$$

Like the Material Removal Rate (MRR) for machining techniques, DR_a can be used to assess the time efficiency of AM technologies. Baumers et al. [22] found that the EBM technology was the fastest AM technique, with a DR_a equal to 0.130 kg/h for the Arcam A1 EBM machine under a full capacity condition. However, in general, the time efficiency of AM technologies is much lower than the MRR of conventional techniques [15,16]. Table 1 summarises the SEC and the overall average values obtained from literature studies in which Ti6Al4V powders had been processed. The SEC values vary over a wide range of between 60 and 375 MJ/kg. All the studies considered one single component or saturation of just the start plate. Therefore, no studies have been conducted to investigate the effect of nesting along the building direction.

An overall analysis of the literature data shown in Table 1 highlights that a certain relationship exists between the SEC values and DR_a. However, this relationship has never been investigated in the literature. Additionally, all the literature studies considered the analysis of energy efficiency during the melting of a bulk material. This study attempts to fill these gaps.

Machine	DR_a (kg/h)	Mean operational power (kW)	SEC (MJ/kg)	Reference(s)
Arcam A1 (Single component)	0.041 *	2.01	176.67	[5,19,22,25–29]
Arcam A1 (Full capacity)	0.128 *	2.22	61.2	[19,22,27,29]
Arcam A1 (Single component)	n.a.	2.01	177	[4,5,20,22,27]
Arcam A1 (Full capacity)	0.130	2.22	61	[4,20,22,27]
Arcam S12 (Full platform)	0.066 *	n.a.	118.46 *	[23]
Arcam A1 (Full capacity)	0.130 *	2.22	59.96	[4,20,24]
Arcam	n/a	n/a	375.0	[4,20,21]

Table 1. SEC data available in the literature for the Electron Beam Melting (EBM) process applied to Ti6Al4V. Full capacity is intended the saturation of just the start plate. The values marked with * have been computed and adapted by the authors of the present paper.

3. Materials and methods

According to the process description presented above, three main subphases can be distinguished: (1) vacuum generation, (2) the building phase and (3) the cooling phase. Process subphase (2) can be further subdivided into: (2.1) beam alignment, (2.2) start plate heating and (2.3) the printing phase. Arcam systems have a specific control that records all the outputs of all the sensors that are present in the machine and monitors the process. The outputs and their time history are saved in an easily accessible log file. The log file was used to extract all the information about the times for the energy consumption calculation. Moreover, according to the electric scheme of Arcam EBM A2x, a decomposition of the machine architecture into its main subunits is carried out as follows: (i) base system of the machine, (ii) vacuum pumps, (iii) high voltage unit, (iv) electron beam, and

(v) rake and build platform. These units are present in the EBM Arcam A2x machine and a chiller unit is connected externally to the machine. The relative energy demand is assessed for each job. The time and the energy efficiency of each job was evaluated for the printing window (2.3) and at the unit process level. The electric energy consumption was measured during all the phases of the EBM process by means of a Fluke 435 Series II analyser. The Arcam A2x EBM machine is powered by an AC three-phase system. The AC current clamps (one for each single AC phase and one for the neutral phase) and the voltage clamps were connected to the electricity supply wires on the EBM machine. The Arcam A2x EBM machine is powered by a current stabiliser, which cleans noises in the power grid and provides the current and voltage phasors with 120 degrees of mutual angular delay as well as a power factor of about 0.95 between the real power and the apparent power. All the current, voltage, power and energy profiles were elaborated using the Fluke Power Log proprietary software. To distinguish the contribution of each unit, the isolated powering of each unit has been considered. The energy demand for each unit is obtained by the additional energy contribution required respect to a reference condition. In details, the power demand of the base system of the machine has been measured evaluating the machine on its standby condition. That measurement was also repeated during the cooling phase, which is characterized by only this machine subunit as well. Then the motor of the rake and the motor of the build platform have been operated manually one per time. Their contributions have been calculated by the differences between the total power demands and the one associated with the stand-by condition. After each job, these contributions have been double checked in the log file of the machine. The contributions have been found to be constant along the building direction and throughout the jobs. The energy demand of the motor of the build platform is around 30% of the rake motor. The total contribution due to the rake and the build platform motors is obtained by multiplying the obtained values for the number of the layers. To measure the contribution of the pumps, from the stand-by condition the pumps have been started up. The vacuum pumps contribution has been quantified by the difference between the overall energy demand during the vacuum generation phase and the one of the base system of the machine. In this condition, the high voltage unit has been activated and its contribution has been calculated by the difference between the overall energy demand and the previously calculated. During the job, the remained energy demand quantity is the one associated with the electron beam.

The ratio between the total job mass and the relative time necessary to complete the job (i.e. the time necessary for the printing window and for the entire process, respectively) was computed to assess the time efficiency. The ratio between the required energy (i.e. the energy necessary for the printing window and for the entire process, respectively) and the total mass was considered to assess the energy efficiency. The mass of each printed job was computed considering the nominal density of the material for the melted volume, for the support and for the lattice parts as well as the relative volumes (see Table 2).

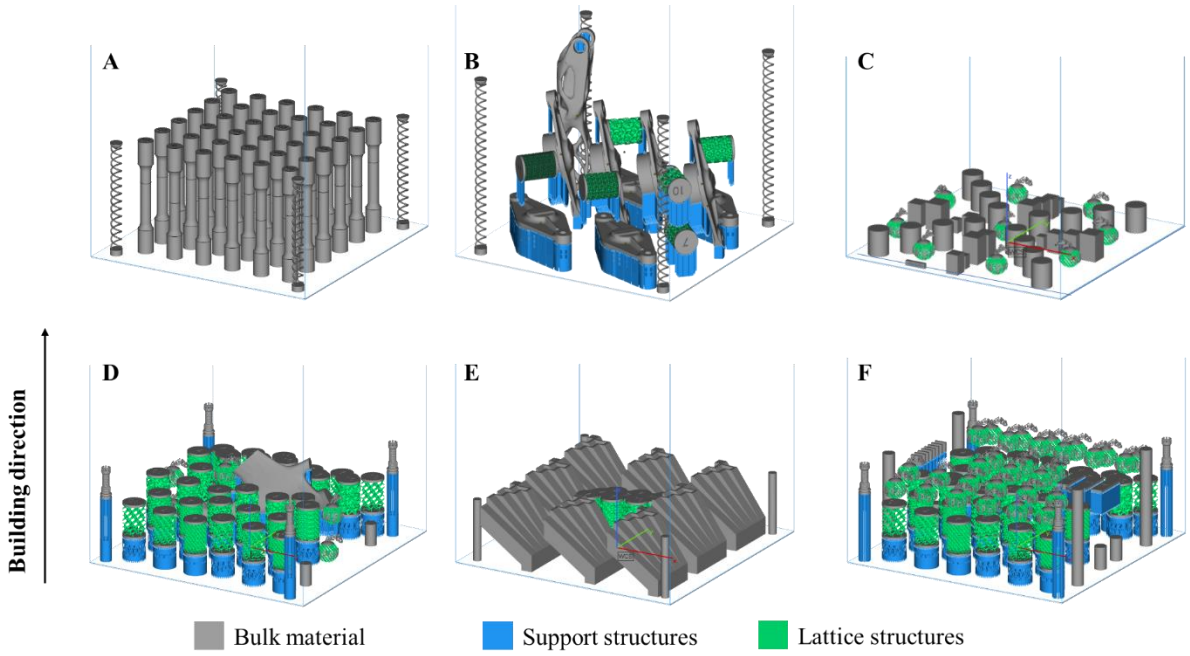

Figure 1. Designed job

Six different job were designed to accurately describe the effects of the part and manufacturing designs (Figure 1). Each part was designed using Solidworks 2018 and was converted into an STL file using the same setting. Job A included the melting of only the bulk material. Job C was designed to analyse the effect of the presence of the bulk material and lattice structure. Jobs B, D, E and F were designed to analyse the effect of the presence of all the themes. Therefore, the bulk, support and lattice structures were all included. Job B was designed to have only the bulk and support materials in the first part of the production. Replicas of the same component were produced in Job B. The replicas were also positioned in two different orientations. The horizontal position was chosen as being representative of a component that is oriented in the worst orientation for the EBM process because a high number of supports needs to be included, there is a great variation between the melted area and non-melted area (support) along the building direction and a low saturation of the building volume. On the other hand, this orientation may be the best orientation from the dimensional and accuracy points of view. Replicas which were oriented at a certain angle with respect to the building direction are representative of a part that is orientated to reduce the number of supports and improve the saturation of the machine. Table 2 shows the geometrical specifications of each job. The build height ranged between 26.82 mm (Job C) and 141.15 mm (Job B). The level of used building volume is the product of the start plate area and the height of the job. This parameter gives information on the overall amount of powder used during the process and it is therefore directly correlated to the job height. The degree of saturation of the build volume (Table 2) is the ratio between the nominal volume (STL volume) and the total amount of powder provided during the job (used building volume). The minimum degree of saturation considered in this study was about 4% for Job B and the maximum was around 11% for Job C. Differences in the degree of saturation allow to analyse the effect of build height and nesting on the SEC values to be evaluated. To evaluate the weight on the energy consumption of the preheating phase, the preheating area was around to 35340 mm^2, except for the Job C, which was 34980 mm^2. Each job was prepared using Magics 21 and processed using Build Processor 2.0. The standard Arcam themes for Ti6Al4V were used. According to that, the layer thickness was set equal to 0.050 mm. The process

parameters are summarised in Table 2. The average beam current was set to 30 mA. The beam current for the support is 5.5mA. The job was produced by an Arcam A2X machine equipped with a standard start plate with 210x210 mm^2 dimensions.

ID	Job height (mm)	Used building volume (cm^3)	Degree of saturation of the build chamber (%)	STL volume (cm^3)	Bulk volume (cm^3)	Support volume (cm^3)	Lattice volume (cm^3)
A	96.08	4237.3	7.75	328.6	328.6	0.0	0.0
B	141.15	6224.9	4.09	254.9	222.4	23.6	8.9
C	26.82	1182.7	11.26	133.2	132.5	0.0	0.7
D	83.27	3672.4	4.35	159.8	84.6	28.0	47.2
E	55.00	2425.5	8.50	206.2	189.7	4.9	11.6
F	87.04	3838.6	4.45	170.7	94.2	26.5	50.0

Table 2. Geometrical specifications of each job.

Process parameter for contour of the bulk						
Melting strategy	Scan speed [mm/s]	Focus Offset [mA]	Beam Current [mA]	Number of spots	Number of contours	Hatch contours [mm]
MultiBeam	850	6	5	70	3	0.29
Process parameter for the hatching for the bulk						
Melting strategy	Speed Function	Focus Offset [mA]	Beam Current Max [mA]	Reference Length [mm]	Reference Current [mA]	Line Offset [mm]
Continuous	45	25	20	45	12	0.2
Process parameter for the outer contour of the lattice						
Melting strategy	Scan speed [mm/s]	Focus Offset [mA]	Beam Current Max [mA]	Number of contours	Hatch contours	
Continuous	450	0	3	1	0.13	
Process parameter for the inner contour of the lattice						
Melting strategy	Scan speed [mm/s]	Focus Offset [mA]	Beam Current Max [mA]	Number of contours	Hatch contours	
Continuous	470	0	3	1	0.13	

Table 3. Process parameters for the melting phase.

4. Results

Figure 2 shows the power profile of the Arcam EBM A2x machine for the manufacturing of Job A. The different process subphases have been subdivided as reported in the methodology section. The chiller unit acquisition has been added to that of the EBM machine for the entire process, from subphase (1) to subphase (3). The chiller is characterised by a duty cycle that ranges from 0.45 kW to 2 kW, as the lower and upper power levels, respectively. The durations of the upper and lower power levels are not fixed but depend on the machine. An average power was computed for each process subphase. In other words, the measured average chiller power demand for process subphase (1) was 720780 W, while a value of 1000 kW was assumed for process subphase (2), since the melting process produces heat that the machine needs to remove in order to maintain an appropriate process temperature. A slightly lower power is registered during the cooling phase, that is, a power of 920 W. The time and energy demand of each process subphase are analysed in the following sections. Furthermore, each machine subunit is characterised.

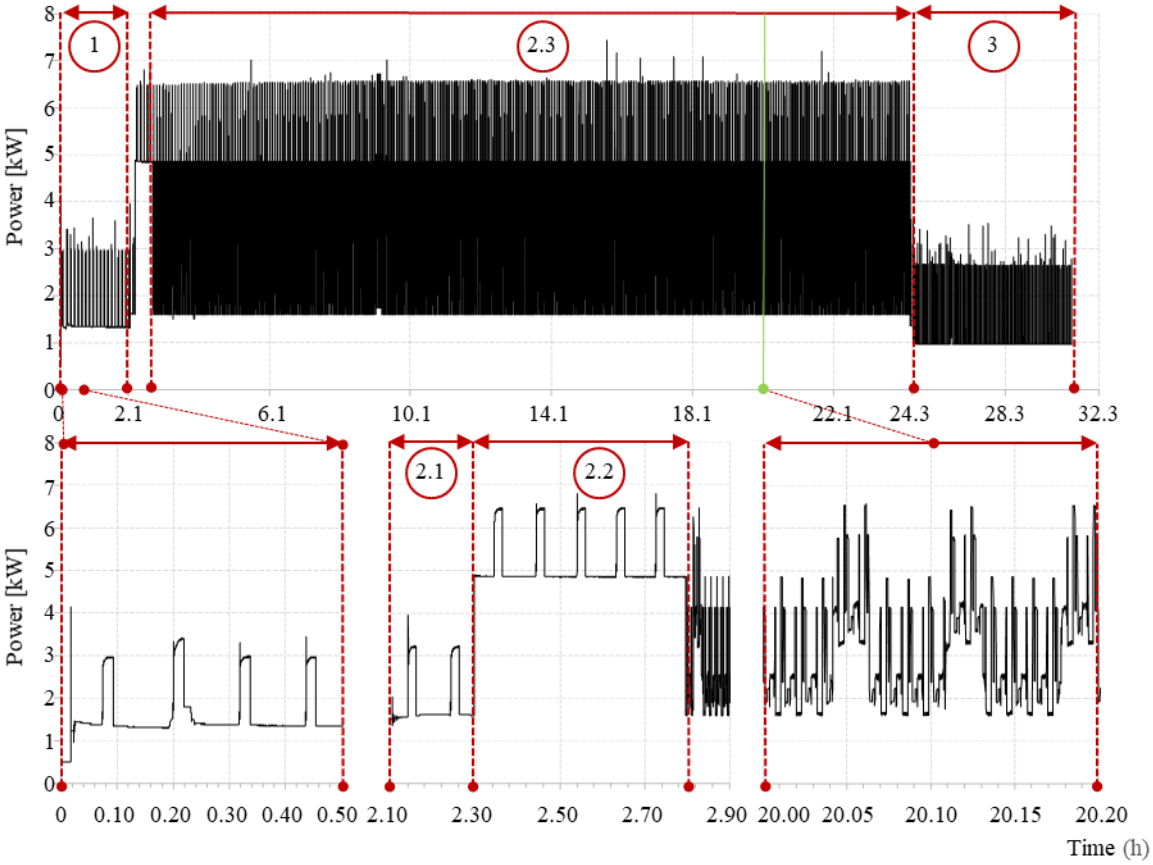

Figure 2. Entire power acquisition for Job A.

4.1 Process subphase (1): Vacuum generation

The vacuum generation subphase starts with the machine set to the idle condition. The relative machine power demand due to the base systems of the machine (i) is 510 W. The operator then starts the vacuum generation procedure. Figure 2 shows a rise in the power demand after about one minute, which is due to the power initialisation of the two vacuum pumps. After their transitory window, the power demand of machine subunit (ii) stabilises at 390 W. Table 4 displays the time and the overall energy (i.e. considering the chiller system) needed to reach a vacuum condition that is suitable to switch on the electron beam. The differences in time can mainly be attributed to the amount of powder in the hoppers for the job that has to be manufactured and the amount of residual powder in the hoppers from the previous job.

Job ID	Process time (h)	Energy demand (MJ)
A	2.1	12.2
B	1.3	7.3
C	1.7	9.9
D	1.1	6.2
E	1.6	9.1
F	1.0	5.9

Table 4. Process time and energy demand results for the vacuum generation.

4.2 Process subphase (2): Build process

Once the machine has reached the vacuum condition, the energy demand is around 900 W, which considers both machine subunits (i) and (ii), plus a power demand of 720 W (which is the average power for a standby condition) for the chiller. The electron beam needs to be switched on manually and this is carried out during process subphase (2.1). The machine activates the high voltage unit (iii) which requires a delta power of 230 W, see Figure 2. Once beam alignment has been achieved, process subphase (2.2) starts. Moreover, the electron beam subunit (iv) is activated during subphases (2.1) and (2.2) with a powered demand that depends on the specific action of the moment. For instance, during process subphase (2.2), the electron beam is powered with up to 3.3 kW to provide the necessary heat to the build table. Table 5 reports the time and energy demand of process subphases (2.1) and (2.2), considering the contribution of the chiller. These phases are not influenced by the job being manufactured since they are related to the internal procedures of the EBM Arcam A2x machine.

Phase	Process time (min)	Energy consumption (MJ)
(2.1) Beam alignment	12.14	1.56
(2.2) Start plate heating	30.00	9.65

Table 5. Build process: Contributions to the process time and electric energy consumption due to the non-printing phases.

Figure 2 shows details of process subphase (2.3) for the manufacturing of several layers together with the duty cycle of the chiller. Figure 3 shows the machine power demand during the printing phase for Job C during the formation of three subsequent layers without the presence of the the chiller. All the machine subunits are powered. The orange, blue and yellow lines depict machine subunits (i), (ii) and (iii) respectively. As described above, the power demand is constant. The power profile for the electron beam (iv) (green line) depends on the specific action. The rake and start plate subunit (v) is depicted in red (Figure 3). The first peak indicates the start plate movement. The three next hills that indicate the three rake movements from one side to the other site to distribute the correct amount of powder onto the previous layer can be seen between each layer. The time necessary to distribute the powder is about 11 sec for each layer. The rake and start plate power demand is negligible, compared with those of the other machine subunits. However, an overall energy demand of 13.40 kJ was considered in this paper regarding the machine subunit (v) for each layer. Machine subunits (iv) and (v) are powered alternatively when the beam is melting and during the spreading of the powder. The trend of the electron beam machine subunit can be further specified by evaluating each melting step, considering Job C (Figure 4). As mentioned in the process description section, the following steps can be observed for each layer during the EBM process: (a) first preheating, (b) second preheating, (c) contouring, (d) melting, (e) support melting and (f) post heating/ cooling.

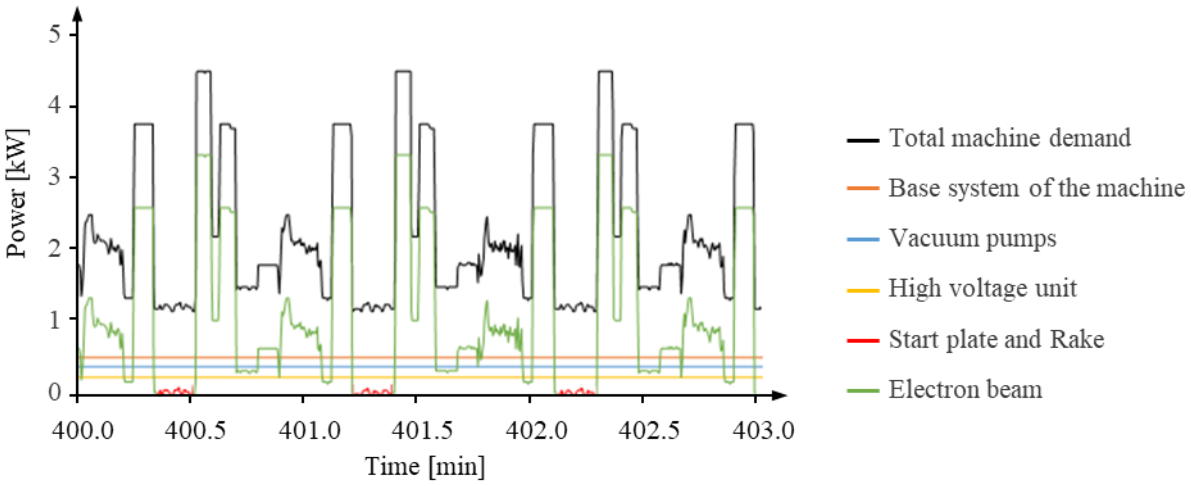

Figure 3. (2.3) Printing phase: data acquisition and identification of the different machine subunits.

During phase (a), a large amount of power is required to heat the preheating area. As in process subphase (2.2), the electron beam is highly defocused and a high amount of power of about 3.3 kW is required. However, a low amount of specific energy is involved in the process because only the sintering of the powder is performed. Phase (b) requires a power demand of 2.5 kW, but only for selected areas on the layer. The duration of this phase appears to depend on the dimension of the subsequent melted area. The necessary specific melting energy is given during phases (c)-(e). The contour consists of two different contours that are melted with the MB strategy. The power demands generally required for the first and second contour strategies can be assumed constant and equal to 0.34 kW and 0.64 kW, respectively (Figure 4). The duration of phase (c) depends on the total length of the perimeters. The melting phase (d) consists of the melting of the bulk area or lattice structures according to the CAD file. The power demand for phase (d) ranges from 0.6 to1.4 kW for the bulk theme. The Arcam A2x control system adjusts the power in order to provide a constant average amount of heat to each layer section being melted. A constant power demand of 0.19 kW is required for the lattice structure, as can be seen in Figure 4. The duration of phase (d) depends on the extension of the overall melted layer area. The support structures are melted during phase (e), with a constant power of 0.37 kW (not shown in Figure 4). The duration of this phase is related to the number of supports in the layer. Finally, the post heating or cooling balances the total heat amount provided for each layer. Therefore, the time and power demand of this phase depend to a great extent on the design of the part and the job (orientation and number of supports).

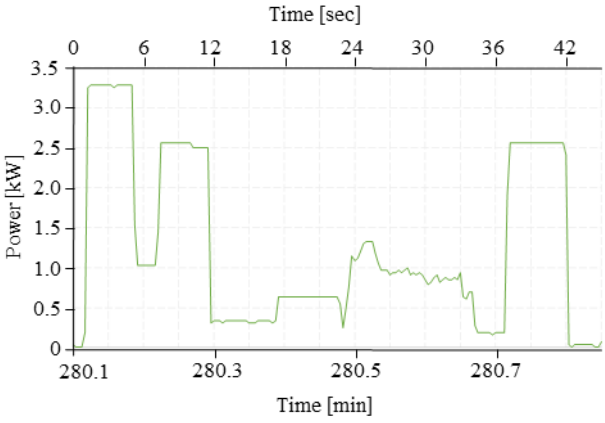

Figure 4. (2.3) Printing phase: data acquisition and identification of the main layer subphases.

Figure 5 reports the overall time (t_{build}) and energy (E_{build}) necessary for each job for process subphase (2). The chiller energy demand is also included. Subphases (2.1), (2.2) and (2.3) are differentiated. Subphase (2.3) dominates the overall energy demand of the build window (2).

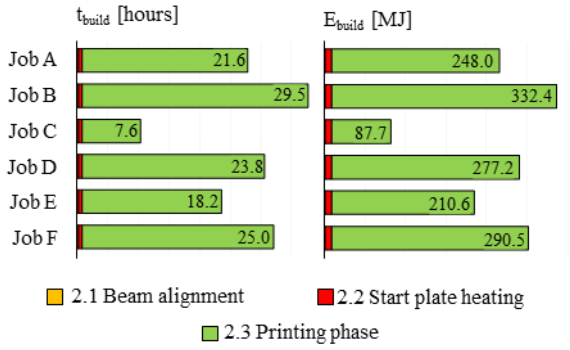

Figure 5. Analysis for the time (t_{build}) (left) and energy demand (E_{build}) (right) for the build process phase.

4.3 Process subphase (3): Cooling

As can be seen in Figure 2, once the job has been completed, the power demands drops because the electron beam, the rake and start plate unit and the vacuum pumps are no longer powered. Only the energy consumption for the machine electronics and the chiller can be observed in this phase. Table 6 presents the time and the energy needed for each job to reach a temperature of 80°C, which is the target temperature necessary to unload the built job. Table 6 shows that the energy demand depends to a great extent on the part and manufacturing designs. The most relevant factor is the job height. However, Job A and Job B have the same cooling time but different build heights. This difference can be explained by considering the total amount of melted material, which is higher for Job B and may therefore lead to a higher temperature in the chamber and a longer cooling time.

Job ID	Process time (h)	Energy demand (MJ)
A	6.8	34.9
B	6.8	34.9
C	2.2	11.9
D	6.1	31.3
E	5.7	29.4
F	6.5	33.2

Table 6. Process time and energy demand for the cooling phase.

5. Modelling

The evaluation of the energy demand of a manufacturing system can be performed at different levels [30]. The modelling methods used at a unit-process level are usually classified as black-box approaches and bottom-up approaches. The former empirically correlate the input process parameters with an output. The latter instead fractionate the output into its contributions from the machine states or subunits [31]. Different applications of these approaches are offered hereafter to describe the unit process energy consumption of EBM.

5.1 Bottom-up approach: energy demand fractionation based on machine states

5.1.1 Energy modelling of the vacuum generation subphase

This phase is characterised by the presence of machine subunits (i) base system of the machine, (ii) vacuum pumps and by the energy consumption related to the chiller. Machine subunits (i) and (ii) show a constant power with respect to time. The chiller energy consumption can be modelled in the same way. Therefore, a linear model such as Eq. (2) can be used.

$$E_{vacuum} = a \cdot t_{vacuum} \qquad (2)$$

where 'a' is the sum of the power of the three powered units. Considering the process time in hours and the energy demand in MJ, the constant 'a' is equal to 5.83 MJ/h. This equation was obtained by interpolating the experimental results reported in Figure 6, which connect the overall measured energy during subphase (1) with the relative process time (see Table 4). A linear regression of the experimental data was carried out using Matlab 2019, which provided a value of constant 'a' equal to 5.83 MJ/h with the confidence interval equal to 95% (5.81-5.85 MJ/h, R^2=0.99).

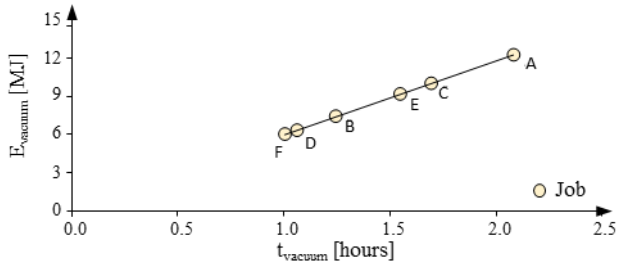

Figure 6. Experimental analysis between energy (E_{vacuum}) and time (t_{vacuum}) for the vacuum generation phase.

5.1.2 Energy modelling of the printing subphase

Subphase (2.3) is characterised by the presence of all the machine subunits. A linear regression between the experimental time and energy results (Figure 5 in green) can be computed by means of Matlab 2019 and fixing a confidence interval equal to 95% (see Eq. 3) as shown in Figure 7.

$$E_{print} = b \cdot t_{print} \qquad (3)$$

where 'b' is equal to 11.51 MJ/h (11.33-11.69 MJ/h, R^2=0.99). The energy demand of the machine subunits (i) base system of the machine, (ii) vacuum pumps and (iii) high voltage unit as well as the chiller is linearly dependent on the time. Even though the machine subunits (iv) electron beam, and (v) rake and start plate do not have a constant power profile with respect to time, Figure 7 shows that a linear model is able to fit the experimental results for subphase (2.3). This trend can be explained as effect of the adjustment on the beam current made by the EBM control to achieve the fixed average beam power over each layer and leads to a constant power. The contribution from the rake and start plate are constant as well.

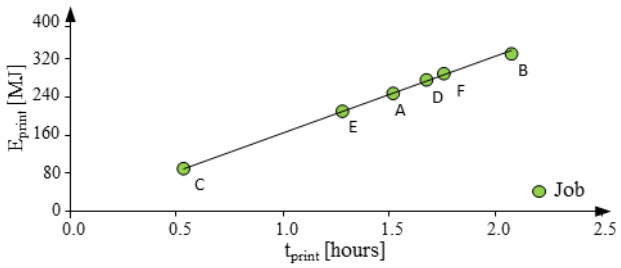

Figure 7. Experimental analysis between energy (E_{print}) and time (t_{print}) for the printing phase.

5.1.3 Energy modelling of the cooling subphase

Subphase (3) is characterised by the presence of machine subunit (i) and the energy consumption related to the chiller. The same approach adopted for process subphase (1) can be applied here, as reported from Eq. (4).

$$E_{cooling} = c \cdot t_{cooling} \qquad (4)$$

where 'c' is the sum of the power of the two powered units. Considering the process time in hours and the energy demand in MJ, the modelled value of constant 'c' is 5.15 MJ/h. In the same way as for subphase (1), a linear regression was obtained between the experimental time and energy results by means of Matlab 2019, fixing an interval confidence equal to 95% (Figure 8), and using the results reported in Table 6. The experimental value of constant 'c' is equal to 5.14 MJ/h (5.10-5.19 MJ/h, R^2=0.99).

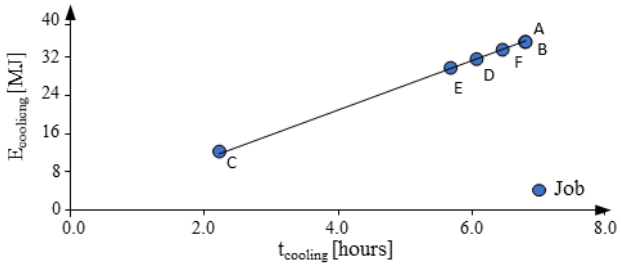

Figure 8. Experimental analysis between energy ($E_{cooling}$) and time ($t_{cooling}$) for the cooling phase.

5.1.4 Unit process level

The principle of superposition can be applied to predict the energy demand of the entire EBM process (Eq. (5)). All the energy demand contributions for the powder bed set up (E_{bed}) or for build chamber cleaning ($E_{cleaning}$), respectively, can be assessed at the beginning and at the end of the EBM process, as having a power demand of 1230 W (which considers machine subunit (i) plus the chiller power demand in its standby condition). The energy demand of process subphase (1), E_{vacuum}, and process subphase (3), $E_{cooling}$, can be assessed as reported in Eq. (2), Eq. (3) and Eq. (4), respectively. The energy involved in process subphase (2) is computed as in Eq. (6). The energy demands for beam alignment ($E_{alignment}$) and start plate heating (E_{table}) are assumed to be constant, according to Table 5.

$$E^{EBM} = E_{bed} + E_{vacuum} + E_{build} + E_{cooling} + E_{cleaning} \qquad (5)$$

$$E_{build} = E_{alignment} + E_{table} + b \cdot t_{print} \qquad (6)$$

Figure 9 and Figure 10 show the process subphase times and energy as percentages of the total demands, respectively. Moreover, process subphase (2.3) is decomposed into the contributions related to the spread of the powder layer (Powder spreading) and that of the melting procedure (Activated EB). The vacuum generation procedure affects the time and energy demands by 3-7% and 2-4% on average. When a small job is considered

(see Job C), the weight of process subphase (1) can reach 14% and 8% of the total time and energy demands, respectively. The beam alignment step and the heating of the start plate have constant time and energy demands. As it is possible to see from Figure 7, their impact on the total time demands is negligible. However, their energy impacts can be comparable with those of the vacuum generation subphase, due to the presence of machine subunit (iv). The printing window accounts for over 60% of the process time in all the cases, with a maximum of 77% for Job B. The energy impact of this phase on the overall demand is even higher (between 72% and 86%), since subphase (2.3) is mainly characterised by the presence of machine subunit (iv). The entities of the powder spreading time and energy are related to the job height (Table 2). As far as the results of this work are concerned, the cumulated time and energy of the coating represent 13-22% and 10-18% of the total time and energy, respectively. Only the machine base system and the chiller are powered during the cooling phase. Therefore, even though this phase can last a long time, its weight on the total energy demand is at least half of that of the total time demand.

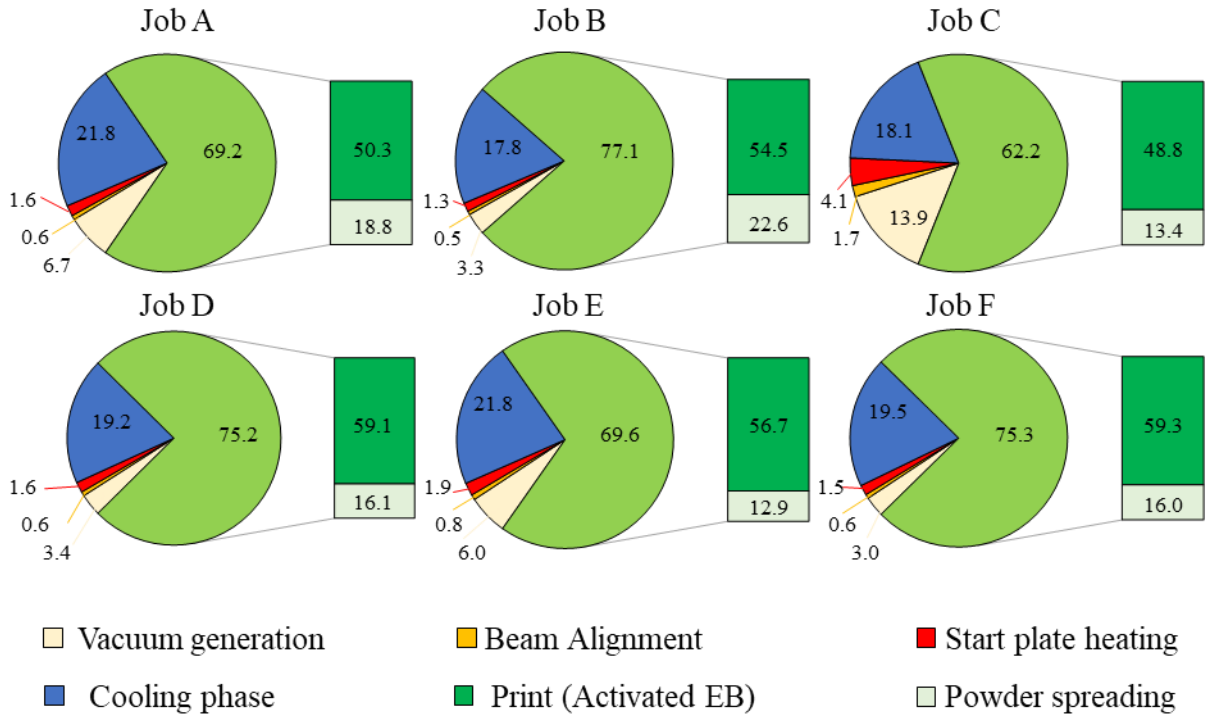

Figure 9. Process subphase times as percentages of the total demand.

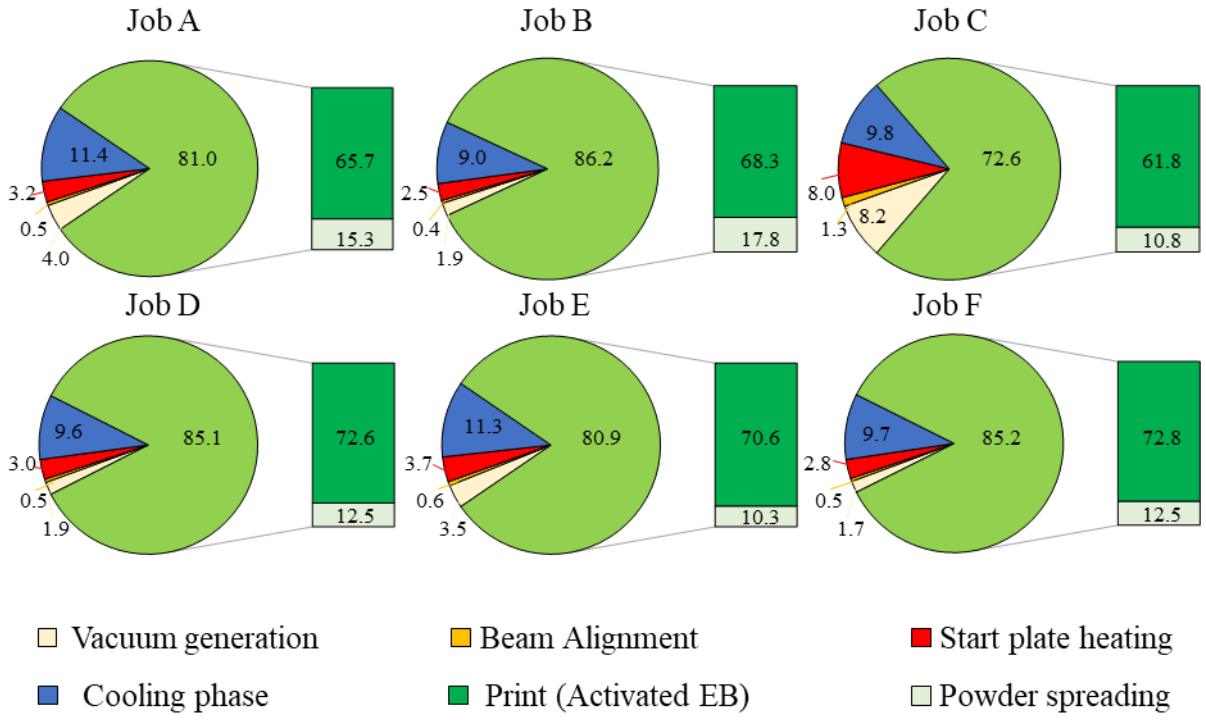

Figure 10. Process subphase energies as percentages of the total demand.

5.2 Empirical approach: time and energy efficiency

As far as the Specific Printing Energy (SPE) is concerned, further considerations can be made on the energy efficiency of the EBM technology by focusing on process subphase (2.3). This parameter is defined as the ratio of the entire energy demand of subphase (2.3), i.e. the printing phase, to the overall printed mass. The mass is calculated using a nominal density of Ti6Al4V of 4.43 g/cm^3 [24]. In order to assess the time efficiency characterisation, the Average Printing Deposition Rate (DR_{aprint}) is evaluated as the ratio between the overall printed mass and the time needed for subphase (2.3). A statistical analysis, performed by means of Matlab 2019, highlighted a hyperbolic law (Figure 11) with an R^2 value equal to 0.99. This result is related to the linear relationship that exits between the E_{print} and t_{print}. As mentioned above, the power demand of all machine subunits is or can be approximated as constant. In fact, e.g., if both terms of Eq. 3 are divided by the mass and expressed as a function of DR_{aprint}, the hyperbolic relationship is obtained as expressed in Eq. (7).

C_{print} is a constant (in MJ/h) and quantifies the average constant power rate resulting from the energy consumption of the different machine subunits which are powered during process subphase (2.3). Its value and the relative 95% confidence interval (Table 7) are in fact close to those of constant b modelled in Eq. (2).

$$SPE = \frac{C_{print}}{DR_{aprint}} \quad (7)$$

Considering Figure 1 and Table 2, it is possible to notice how jobs characterised by the presence of lattice structures and supports (D and F) slow down the deposition efficiency. The jobs that are mainly composed of melted volumes (A and C) show the highest deposition efficiency. If only the effect of the bulk material theme is considered, jobs with a greater height (such as Job B) have a lower DR_{aprint} than shorter jobs (such as job C) since powder spreading is a not an active phase. If the deposited mass change (meaning a change in the job

design), the new SPE and DR_{aPrint} values will still belong to the same curve. This result is typical for processes which are dominated by constant power, that is, with energy requirements that scaled with the time [32].

At the unit process level, the SEC parameter and the overall Average Deposition Rate (DR_a), as defined in the introduction section can be considered. As before, the experimental analysis showed a hyperbolic law between these two variables (Figure 11 and Eq. (8) with an R^2 value equal to 0.99).

$$SEC = \frac{C_{EBM}}{DR_a} \qquad (8)$$

Where C_{EBM} is a constant expressed in MJ/h (Table 7). Significant increase of SEC can be observed for lower DR_a, while for the higher DR_a values, the SEC stabilizes itself, reflecting relatively SEC reduction for higher DR_a values. The meaning of both C_{print} and C_{EBM} is thus connected closely to the process control and machine architecture. The value of C_{Print} is higher than that of C_{EBM} because the non-printing phase lowers the overall energy consumption. The SEC-DR_a curve is moved to a lower time and energy efficiency position, with respect to the SPE-DR_{aprint} curve. As previously mentioned, the print phase (2.3) dominates all the time and energy demands. A similar trend is in fact observed if the printing phase or the unit process level is taken into consideration. Both curves depend directly on the architecture of the machine and the process control. In fact, even when a wide variation of input parameters is considered, all the results lie on the same hyperbolic curve. Each input variable affects the time efficiency, which is holistically described by the average Deposition Rate. In this sense, as far as the energy efficiency characterisation of the EBM process is concerned, the complexity affects the SEC value, and a complex job has features that can slow down the average Deposition Rate (such as supports or small melting areas, as in the case of a lattice structure).

C_{print} [95% confidence bounds]	11.56 [11.40, 11.72]
C_{EBM} [95% confidence bounds]	10.16 [9.97, 10.36]

Table 7. Value of the constants for the hyperbolic laws, expressed in MJ/h

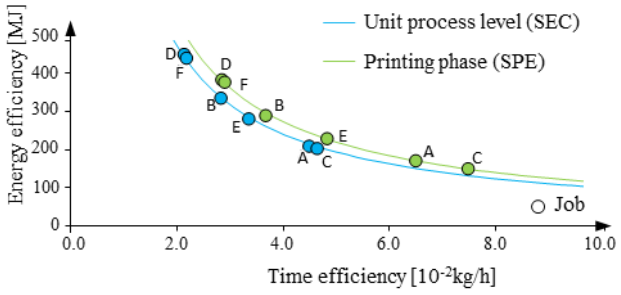

Figure 11. Time and energy efficiency of the printing process subphase (Eq.7) and at a unit process level (Eq.8).

5.3 Bottom-up approach: energy demand fractionation based on the machine subunits

Figure 12 shows the energy (in MJ) consumed by each subunit of the machine during the entire EBM process, i.e. considering process subphases (1), (2) and (3). For the sake of clarity, the constant power demands of machine subunit (i), (ii) and (iii) as well as those of the chiller are reported in Table 8. Table 9 shows the average values of the energy demand of each subunit of the machine as a percentage of the total energy demand and the relative standard deviation. The interesting result is that similar proportions are maintained for the

energy demands of the different subunits for each job. In fact, the results of the standard variations do not affect the magnitude of the average computed values. As previously discussed, the energy demand of the rake and start plate is negligible, because it is related to 0.52% of the total energy demand. The chiller system is the highest energy consumption unit, with a value of 34.64%. This unit is followed by the electron beam (29.28%). Then, the base system of the machine, the vacuum pumps and the high voltage unit follow with 18.27%, 11.21% and 6.08 %, respectively. A further reflection can be made considering that only 29.28% of the total energy demand is needed for the Arcam EBM A2x machine for the melting procedure. Instead, 70.72% of the total energy demand is needed to make the melting procedure possible. Therefore, the optimisation of the energy efficiency of the EBM technology requires not only the optimisation of the additive process, but also that of the machine subunits.

Phase	Power demand [W]
Base system of the machine, P_i	510
Vacuum pumps, P_{ii}	390
High voltage unit, P_{iii}	230
Chiller average power during subphase (1), (P_{C1})	720
Chiller average power during subphase (2), P_{C2}	1000
Chiller average power during subphase (3), P_{C3}	920

Table 8. Constant power demand of machine subunits (i), (ii) and (iii) and of the chiller.

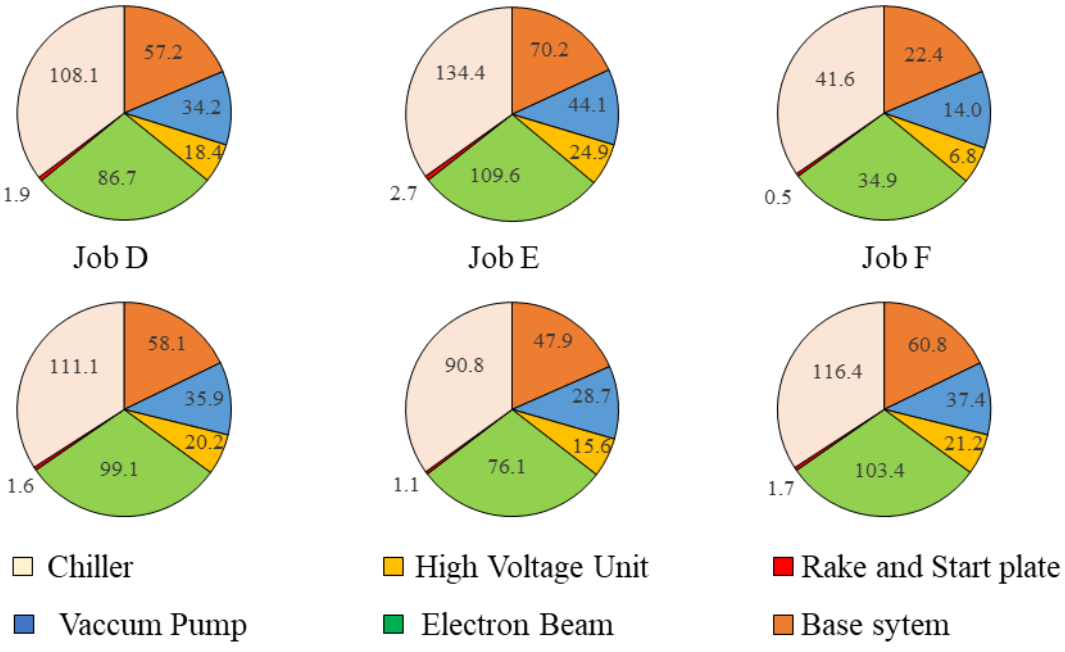

Figure 12. Unit process energy consumption results (in MJ) divided by the machine subunits.

Phase	Average %	Standard deviation in %
Machine base system	18.27	0.38
Vacuum pumps	11.21	0.28
High voltage unit	6.08	0.27
Electron beam	29.28	0.91

Rake and start plate	0.52	0.11
Chiller	34.64	0.46

Table 9. Constant power demand of machine subunits (i), (ii) and (iii) and of the chiller.

6. Conclusions

SEC is a well-known parameter that has been used in literature to assess the energy efficiency of different technologies at the unit process level, while DR_a can be used to evaluate the time efficiency of additive techniques. In this paper, the relationship between these two factors has been investigated for the EBM process considering different part and manufacturing designs. The effects on the energy efficiency of all the process themes (bulk material, supports and lattice structures) available for the EBM process, the job heights, the nesting along the building direction and the degrees of saturation of the build volume have been investigated. The main finding of the study has been the identification of a hyperbolic variation law between time efficiency and energy efficiency. This law is closely correlated with the architecture of the machine and the process control. In fact, even when such a wide variation of input parameters is provided, in terms of design, all the results lie on the same hyperbolic curve, which can be computed at the unit process level or for the printing window (2.3). Each input variable affects the time efficiency, which is holistically described by the average Deposition Rate. From this point of view, the complexity of EBM systems can be represented by the design complexity, which includes the use of supports or small melting areas, as in the case of a lattice structure.

These results represent a step forward in the energy characterisation of AM technologies, and open the way towards a wide application of the presented methodology to characterise AM machines and to obtaining a better understanding of the dispersion of SEC values that are currently available in the literature.

References

[1] A. 52900:2015, Standard Terminology for Additive Manufacturing – General Principles – Terminology, ASTM Int. i (2015) 1–9. https://doi.org/10.1520/F2792-12A.2.

[2] M. Galati, L. Iuliano, A literature review of powder-based electron beam melting focusing on numerical simulations, Addit. Manuf. 19 (2018). https://doi.org/10.1016/j.addma.2017.11.001.

[3] L.U. Larsson Morgan, H. Ola, Rapid manufacturing with electron beam melting (EBM)—A manufacturing revolution?, Solid Free. Fabr. Symp. (2003) 438–443.

[4] K. Kellens, M. Baumers, T.G. Gutowski, W. Flanagan, R. Lifset, J.R. Duflou, Environmental Dimensions of Additive Manufacturing. Mapping Application Domains and Their Environmental Implications, Environ. Dimens. Addit. Manuf. 3D Print. 21 (2017) S49–S68. https://doi.org/10.1111/jiec.12629.

[5] H.S. Yoon, J.Y. Lee, H.S. Kim, M.S. Kim, E.S. Kim, Y.J. Shin, W.S. Chu, S.H. Ahn, A comparison of energy consumption in bulk forming, subtractive, and additive processes: Review and case study, Int. J. Precis. Eng. Manuf. - Green Technol. 1 (2014) 261–279. https://doi.org/10.1007/s40684-014-0033-0.

[6] P.C. Priarone, G. Ingarao, Towards criteria for sustainable process selection : On the modelling of pure subtractive versus additive / subtractive integrated manufacturing approaches, J. Clean. Prod. 144 (2017) 57–68. https://doi.org/10.1016/j.jclepro.2016.12.165.

[7] W. He, W. Jia, H. Liu, H. Tang, X. Kang, Y. Huang, Research on preheating of titanium alloy powder in electron beam melting technology, Xiyou Jinshu Cailiao Yu Gongcheng/Rare Met. Mater. Eng. 40 (2011) 2072–2075.

[8] M. Galati, A. Snis, L. Iuliano, Experimental validation of a numerical thermal model of the EBM process for Ti6Al4V, Comput. Math. with Appl. (2018).

[9] J. Karlsson, T. Sjögren, A. Snis, H. Engqvist, J. Lausmaa, Digital image correlation analysis of local strain fields on Ti6Al4V

manufactured by electron beam melting, Mater. Sci. Eng. A. (2014). https://doi.org/10.1016/j.msea.2014.09.022.

[10] Mahale, ELectron Beam Melting of Advanced Materials and Structures, mass customization, mass personalization, 2009.

[11] M. Galati, A. Snis, L. Iuliano, Powder bed properties modelling and 3D thermo-mechanical simulation of the additive manufacturing Electron Beam Melting process, Addit. Manuf. 30 (2019) 100897. https://doi.org/10.1016/J.ADDMA.2019.100897.

[12] E. Attar, Simulation of Selective Electron Beam Melting Processes, 2011.

[13] N.A. Fleck, V.S. Deshpande, M.F. Ashby, Micro-architectured materials: Past, present and future, Proc. R. Soc. A Math. Phys. Eng. Sci. 466 (2010) 2495–2516. https://doi.org/10.1098/rspa.2010.0215.

[14] M. Galati, P. Minetola, G. Rizza, Surface Roughness Characterisation and Analysis of the Electron Beam Melting (EBM) Process, Materials (Basel). 12 (2019) 2211. https://doi.org/10.3390/ma12132211.

[15] S. Kara, W. Li, Unit process energy consumption models for material removal processes, CIRP Ann. - Manuf. Technol. 60 (2011) 37–40. https://doi.org/10.1016/j.cirp.2011.03.018.

[16] Li, W., Sami, K., An empirical model for predicting energy consumption of manufacturing processes: A case of turning process, Proc. Inst. Mech. Eng. Part B J. Eng. Manuf. 225 (2011) 1636–1646. https://doi.org/10.1177/2041297511398541.

[17] A. Thiriez, An environmental analysis of injection molding, Massachusetts Institute of Technology, 2006.

[18] D. Baffari, A.P. Reynolds, A. Masnata, L. Fratini, G. Ingarao, Friction stir extrusion to recycle aluminum alloys scraps: Energy efficiency characterization, J. Manuf. Process. 43 (2019) 63–69. https://doi.org/10.1016/j.jmapro.2019.03.049.

[19] R.W. M. Baumers, C. Tuck, R. Hague, I. Ashcroft, A comparative study of metallic additive manufacturing power consumption, in: 21st Annu. Int. Solid Free. Fabr. Symp. - An Addit. Manuf. Conf. SFF 2010, 2010: pp. 278–288.

[20] K. Kellens, R. Mertens, D. Paraskevas, W. Dewulf, J.. Duflou, Environmental Impact of Additive Manufacturing Processes : Does AM contribute to a more sustainable way of part manufacturing?, Procedia CIRP. 61 (2017) 582–587. https://doi.org/10.1016/j.procir.2016.11.153.

[21] H. Paris, H. Mokhtarian, E. Coatanéa, M. Museau, I.F. Ituarte, Comparative environmental impacts of additive and subtractive manufacturing technologies, CIRP Ann. - Manuf. Technol. 65 (2016) 29–32. https://doi.org/10.1016/j.cirp.2016.04.036.

[22] M. Baumers, C. Tuck, R. Wildman, I. Ashcroft, R. Hague, Energy inputs to additive manufacturing: does capacity utilization matter?, in: 22nd Annu. Int. Solid Free. Fabr. Symp. - An Addit. Manuf. Conf. SFF 2011, 2011: pp. 30–40.

[23] M. Baumers, P. Dickens, C. Tuck, R. Hague, The cost of additive manufacturing: machine productivity, economies of scale and technology-push, Technol. Forecast. Soc. Chang. 102 (2016) 193–201. https://doi.org/10.1016/j.techfore.2015.02.015.

[24] M. Baumers, C. Tuck, R. Wildman, I. Ashcroft, R. Hague, Shape Complexity and Process Energy Consumption in Electron Beam Melting A Case of Something for Nothing in Additive Manufacturing ?, 00 (2016) 1–11. https://doi.org/10.1111/jiec.12397.

[25] M. Baumers, C. Tuck, R. Wildman, I. Ashcroft, E. Rosamond, Transparency Built-in Manufacturing, 17 (2012). https://doi.org/10.1111/j.1530-9290.2012.00512.x.

[26] F. Le Bourhis, O. Kerbrat, J. Hascoet, P. Mognol, Sustainable manufacturing: Evaluation and modeling of environmental impacts in additive manufacturing, Int. J. Adv. Manuf. Technol. 69 (2013) 1927–1939. https://doi.org/10.1007/s00170-013-5151-2.

[27] R. Huang, M. Riddle, D. Graziano, J. Warren, S. Das, S. Nimbalkar, J. Cresko, E. Masanet, Energy and emissions saving potential of additive manufacturing : the case of lightweight aircraft components, J. Clean. Prod. 135 (2015) 1559–1570. https://doi.org/10.1016/j.jclepro.2015.04.109.

[28] M. Yosofi, O. Kerbrat, P. Mognol, Energy and material flow modelling of additive manufacturing processes, Virtual Phys. Prototyp. 13 (2018) 83–96. https://doi.org/10.1080/17452759.2017.1418900.

[29] O. Kerbrat, F. Le Bourhis, P. Mognol, J.-Y. Hascoët, Environmental Impact Assessment Studies in Additive Manufacturing, 2016. https://doi.org/10.1007/978-981-10-0606-7_2.

[30] J.R. Duflou, J.W. Sutherland, D. Dornfeld, C. Herrmann, J. Jeswiet, S. Kara, M. Hauschild, K. Kellens, Towards energy and resource efficient manufacturing: A processes and systems approach, CIRP Ann. - Manuf. Technol. 61 (2012) 587–609. https://doi.org/10.1016/j.cirp.2012.05.002.

[31] Y. Guo, J.R. Duflou, J. Qian, H. Tang, B. Lauwers, An operation-mode based simulation approach to enhance the energy conservation of machine tools, J. Clean. Prod. 101 (2015) 348–359. https://doi.org/10.1016/j.jclepro.2015.03.097.

[32] T. Gutowski, S. Jiang, D. Cooper, G. Corman, M. Hausmann, J.A. Manson, T. Schudeleit, K. Wegener, M. Sabelle, J. Ramos-Grez, D.P. Sekulic, Note on the Rate and Energy Efficiency Limits for Additive Manufacturing, J. Ind. Ecol. (2017). https://doi.org/10.1111/jiec.12664.